Modeling Spin-Precessing Neutron Star Binaries: A Generalization of Black Hole Binary Frameworks in `Precession`
2026 LIGO SURF Proposal

Quinn Kasdan-Grollo, Giulia Fumagalli, and Taylor Knapp
(Dated: July 8, 2026)

I. INTRODUCTION

A current challenge the LIGO/Virgo/KAGRA (LVK) collaboration faces is determining the nature of sources detected with gravitational-waves (GWs). When LVK detects GWs it requires predictions of binary black hole (BH) and neutron star (NS) waveforms to extract a GW signal against background noise – a method called matched filtering [1]. In order to accurately distinguish signal from background via matched filtering, we require highly accurate theoretical waveform templates, which in turn allow us to infer accurate descriptions of the source and its properties. By improving waveform templates, LVK can make the most of GW detections. In order to do this, it is imperative to model the evolution of these binaries from their initial orbits down to the inspiral phase where LIGO can actually detect the emitted GWs.

Moreover, we are unsure how compact binary coalescence (CBC) systems actually form. Through accurate evolutions of CBCs we can match formation models with observations, allowing us to more accurately extract information from LVK detections, and constrain formation channels for CBCs.

While our understanding of binary black holes (BBHs) and their orbital evolution under different initial conditions has improved significantly, we remain in need of better models of NS binaries. This is primarily due to the highly complicated, and still not understood, equation of state of NSs. In this project, we aim to build on the work presented in Ref. [2] by creating accurate and computationally cost-effective models of precessing NS binaries.

II. BACKGROUND

A. Gravitational Waves and Compact Binary Coalescence

Gravitational waves, as predicted by Albert Einstein's theory of General Relativity, are ripples in spacetime produced by massive objects accelerating through the fabric of spacetime [3]. The faster and more massive the object, the more pronounced the ripples – analogous to a motorboat creating larger waves than a duck moving across a pond. GWs, though, are quite hard to detect, despite distorting space they have no noticeable effect on Earth. Thus, to detect GWs we focus our attention to the most massive and relativistic sources – compact binaries and compact binary coalescence. Compact binaries are binary systems consisting of BHs and/or NSs. Initially, the compact objects orbit each other at high speeds, emitting weak GWs that reduce the total angular momentum and orbital energy of the system. Due to this loss of angular momentum and energy, their orbital separation decreases as their orbital velocities increase, eventually initiating an inspiral and merger. In Figure 1 the evolution of a compact binary is shown compared to the predicted strain on a detector. For this project we will focus our attention on the inspiral phase as that is where the key post-Newtonian (PN) approximations used to model the inspiral phase can safely be applied.

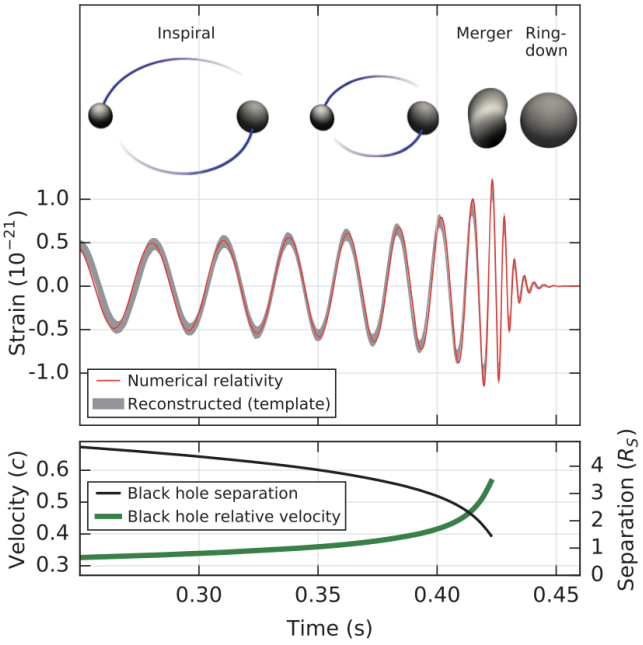


FIG. 1. The predicted strain detected by LIGO from GW150914 – the first detected GW – over inspiral to merger to ring-down as a function of time. Also displayed is the velocity (v/c) compared to the orbital separation [4].

B. Spin-Induced Precession

Compact objects can spin which, as predicted by General Relativity, drags the space-time around them. In binary systems, this space-time dragging can affect the orbit

and spin of the system through spin-orbit and spin-spin couplings. This causes the orbital plane and spins of the compact objects to precess, resulting in precession of the orbital angular momentum vector $\mathbf{L}$ and spin vectors of $\mathbf{S}_1$ and $\mathbf{S}_2$ as seen in Figure 3. These effects modulate the emitted gravitational signal, as first studied by Apostolatos *et al.*. In the absence of precession the predicted waveform monotonically increases until merger, this increase in amplitude is a result of the faster and faster inspiral as the objects close in on each other. Meanwhile, the monotonicity of this increase is due to the dependence of the waveform's amplitude on the geometry of the orbit relative to the detector – as described by Equation 7a in Ref. [5]. Since the orbit is non-precessing, the amplitude increases monotonically. However, in a precessing binary the wobbling of the orbital plane creates a modulating amplitude over time due to $\mathbf{L}$'s time dependence – Equation 19a in Ref. [5]. This modulation of the waveform makes tracking the precessional behavior of compact binaries incredibly important for matched filtering, especially as detectors become more to sensitive GW signals. A comparison of non-precessing and precessing waveforms is shown in Figure 2.

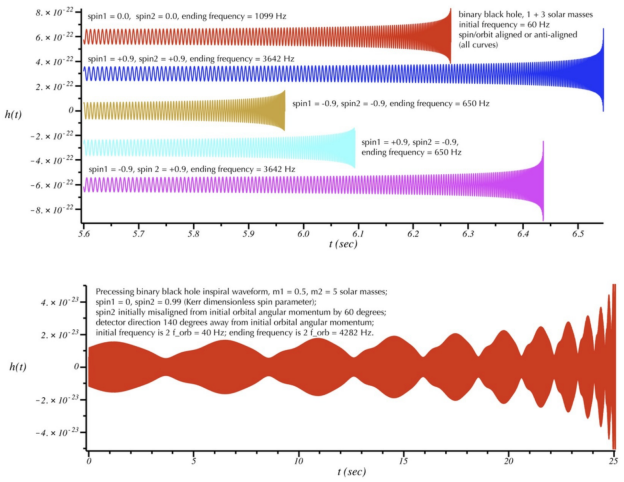


FIG. 2. *Top:* Waveforms of different non-precessing binaries for a range of inital conditions. Note all spins are equal in magnitude and aligned or anti-aligned. The waveform is a plot of predicted detector strain, $h(t)$, over time. *Bottom:* Waveform for a precessing binary showing strain vs. time. Notice how "envelopes" grow and shrink over time but the overall amplitude of the waveform grows as the binary inspirals to merger, this is the direct effect of precession and its modulation of the waveform. Also note the misalignment of the second spin vector with the orbital angular momentum vector by 60^o, hence the induced precession [6].

How precession arises is from the geometry of the spin and momentum vectors in the binary. Let the spin vectors of compact objects 1 and 2 be $\mathbf{S_1}$ and $\mathbf{S_2}$, respectively, and the system's total spin, $\mathbf{S}$, be defined as $\mathbf{S} = \mathbf{S_1} + \mathbf{S_2}$. When $\mathbf{S}$ is misaligned with $\mathbf{L}$ the system will precess. That is, if $\mathbf{S}$ is not parallel or anti-parallel to $\mathbf{L}$, precession occurs. This precession occurs about the systems total angular momentum vector, $\mathbf{J}$, defined as $\mathbf{J} = \mathbf{S} + \mathbf{L}$. A useful graphic showing these vectors can be found in Figure 3. In summary, due to spin-orbit vector misalignment, precession can occur which has a profound impact on the waveform, making it an important property to understand.

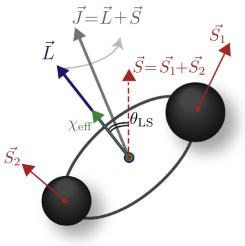


FIG. 3. From Ref. [7] this graphic gives a clear look at the different angular momentum vectors in a spinning binary system as described in Sec. II B. along with $\chi_{\rm eff}$ and θ_{LS} – the effective spin and the spin-orbit misalignment angle, respectively.

C. Modeling Binary Black Hole Orbits

In order to evolve any CBC, we need to account for the effects of General Relativity. While solving Einstein's equations with numerical relativity is the most accurate way to do so, in practice it is incredibly computationally expensive and time-consuming. Instead, we turn to PN approximations to Einstein's equations to model orbital motion, which are accurate to large enough orbital separations ($r > 10M$), and small enough velocities ($v/c \ll 1$) that for our purposes we can avoid the use of costly super-computing. As worked out in Ref. [5], we can use PN spin precession equations to simplify calculations and model the evolution of these systems efficiently. Luckily for us, these approximations are "unreasonably effective" as Will puts it.

Post-Newtonian approximations alone, though, do not get us far enough. While a faster problem to solve than through numerical relativity, the PN approximation still leaves us with a multi-dimensional problem to solve. Instead of dealing with this complex problem, a hierarchal timescale analysis can be used to reduce this to a one-dimensional problem. Gerosa *et al.* lay this out clearly in the first paper outlining the `Precession` code used to evolve BBHs, which we will build on for NS binaries. The timescale hierarchy is $t_{\rm orb} \ll t_{\rm pre} \ll t_{\rm rad}$: the objects' orbital periods are much shorter than the precessional period of the orbital plane, which is much shorter than the duration it takes for the orbital separation to decay due to gravitational radiation by a significant amount.

Gerosa *et al.* improved the methods used in Ref. [9] for

evolving spinning BBHs by implementing precession-averaging to the BBH dynamics. This leaves us with a high-dimensional problem describing the orientations and magnitudes of the spin and angular momenta vectors. This problem relies on seven variables: the mass ratio q, the spin magnitudes χ_1, and χ_2, compacted orbital separation and asymptotic angular momentum terms u and κ, the effective spin $\chi_{\rm eff}$, and the weighted spin difference $\delta\chi$ [2]. On the precessional timescale, five of these are constant: q, χ_1, χ_2, , u, and κ. Due to some special properties of BH spin precession equations – as discussed in Ref. [10] – we also find $\chi_{\rm eff}$ to be a constant of motion on the precessional timescale [2], leaving us with one changing variable on the relevant timescale – $\delta\chi$. In identifying these constants of motion, the previously 7-dimensional problem has been reduced to a 1-dimensional one. Now, with this much simpler analytical treatment of the precessional dynamics, we can average the precessional behavior over a precession cycle, $t_{\rm prec}$. With this average, Equations 61 and 62 in Ref. [2] – which store all the needed information about the binary, such as spin directions – allow us to integrate from some initial orbital separation to a final separation. This integration is of a simple ordinary differential equation, an equation dependent on a single variable, making it extremely easy to work with and compute. By integrating Equation 61 of Ref. [2], the spin-orbit configuration encoded in Equation 14 of Ref. [2] is determined as a function of orbital separation, thus giving us a full evolution of the momentum vector orientations from arbitrarily large separations to separations close-to-merger, where the PN approximation breaks down.

As described, all of this work with BBHs relies on a key constant of motion in the spin precession equations at 2PN, $\chi_{\rm eff}$. When working with NSs, $\chi_{\rm eff}$ is not constant on the precessional timescale [11], thus the methods used in Ref. [2] to evolve BBH spins are invalid for NSs. While in the BH case we can solve a singular equation analytically, in the NS case we are tasked with solving a system of coupled equations numerically, many times, to precession-average (and thus evolve) their orbits. In our project, we will utilize new spin precession equations developed by Giulia Fumagalli generalized to non-BH objects to evolve NS binaries, with the final goal of extending `Precession` to work with NS binaries.

III. OBJECTIVES

Our overall objective is to generalize `Precession` to any precessing CBC evolution, namely for NS binaries. In doing so we seek to understand how spin directions evolve and see how they differ from the BH case. To do this, we must first extend the BH precession-averaging approach used in Ref. [2] to NSs. This has been the main focus of our work so far, and will be described further in Section IV. With a way to precession-average NS binaries, we will implement our findings in a functioning framework and validate our developments against real events. With this, we aim to improve future template matching and contribute to future understanding of CBC formation systems through accurate spin evolution models.

IV. APPROACH

In order to recreate the double-averaging approach that Gerosa *et al.* uses, and ultimately expand upon `Precession`, we take the following steps:

- *Literature review and theoretical setup*: I have read up on existing literature regarding spin precession in CBC, learning about the main difference between BH and NS systems. The main difference arises in the spin-induced quadrupole moment Q:

$$Q_i = -k_i \chi_i^2 M^3 \tag{1}$$

  which characterizes $\mathbf{L}, \mathbf{S}_1$, and $\mathbf{S}_2$. Here M is the total mass of the binary $M = m_1 + m_2$, χ_i is the dimensionless kerr parameter of object i, and k_i depends on the internal structure of the object. While for BHs $k_i = 1$, for NSs the internal structure is poorly constrained and typically have $k_i \sim 2-14$. When k_1 and k_2 equal 1, as in the BH-BH case, the aforementioned $\chi_{\rm eff}$ is constant on $t_{\rm pre}$, for other $k_i \neq 1$ cases, Giulia Fumagalli finds a generalized quantity $\chi_{\rm cons}$ that remains constant on $t_{\rm pre}$ while also reducing to $\chi_{\rm eff}$ in the BH-BH case. Using $\chi_{\rm cons}$ we approach precession averaging similar to Gerosa *et al.*. By finding the roots of $\frac{d\delta\chi}{dt}$ we determine the precessional behavior of $\delta\chi$ (essentially establishing the precessional cone drawn out over $t_{\rm pre}$), encoding all the information about spins and spin-alignment of interest over t_{pre}. If we could accurately find the roots of $\frac{d\delta\chi}{dt}$ we could continue nicely, but currently finding these roots is inefficient and sometimes non-determinate.

- *Learning the basics of* `Precession`: I have familiarized myself with the existing framework for BH-BH binaries by performing inspiral calculations on random initial BH-BH conditions using `Precession`. Furthermore, I learned to propagate posterior samples of BBH initial conditions through `Precession` and compare the final distributions of the binary parameters to the initial distributions, checking that quantities such as χ_1, χ_2, and q stay conserved as expected. Eventually, we hope to do a similar process for NS-NS and NS-BH binaries with our extended version of `Precession` to check its accuracy.

- *Implementation of new equations and root-finding*: Starting from Giulia Fumagalli and Taylor Knapp's preliminary extension of the `Precession` code, we have been investigating efficient ways to find roots

to $\frac{d\delta\chi}{dt}$. In order to simplify some things we actually find the physically meaningful roots of:

$$\frac{d\delta\chi}{dt}^2 = \mathcal{A}^2 \sin^2(\theta_1) \sin^2(\theta_2) \sin^2(\Delta\Phi) \tag{2}$$

by evaluating the roots of a cubic spline fit to the function, as there is no analytical solution for the roots. Although finding the roots of this equation was already set up in the code, Giulia Fumagalli found analytical solutions to the $\mathcal{A}^2, \sin^2(\theta_1)$, and $\sin^2(\theta_2)$ terms, so we investigated if finding the roots of only $\sin^2(\Delta\Phi)$ with a cubic spline and then combining those roots with the analytical roots of the other functions would be more efficient. Results of this implementation, along with additional approaches to root finding will be further discussed in Section V. A further challenge is in higher q and k_i limits, we find that there is a sort of bifurcation where two sets of valid $\delta\chi$ roots are found defining separate, valid precessional cones. After optimizing root finding under the no-bifurcation case, understanding how to approach the bifurcation case will be the next central challenge of this project.

- *Code development*: Once these issues have been dealt with, we will integrate our optimized techniques in a new version of `Precession` extending it to deal with generic CBC spin-precession.

- *Testing and validation*: Afterwards, the code will be tested across a range of physical parameters, including masses, spin magnitudes, orbital separations, and NS equations of state. We will validate the implementation by comparing appropriate limits with known BH results.

- *Application to real events*: Finally, we will apply the developed framework to GW observations of NS binaries, with the goal of reconstructing their spin evolution and connecting measurable quantities, such as spin directions measured by LIGO, to their value at the formation of the binary.

V. INTERIM PROGRESS AND RESULTS

As mentioned in Section IV, we began by looking into ways to speed up root-finding in cases that do not lead to a bifurcation. To do so I set up 1000 initial binary NS scenarios by sampling from an isotropic distribution of masses, spins, and spin-alignment angles and then I found the roots of each term in Equation (2), a particularly helpful finding was that the pre-factor $\mathcal{A}^2$ never contributes a physically meaningful root, thus we know there is no need to include it when evaluating the roots of Equation (2). Figure 4 shows the number of roots from each term, as can be seen in the fourth row $\mathcal{A}^2$ has 0 roots for all 1000 scenarios.

Figure 4 also reveals a few more important points of investigation. Firstly, the second to last row of the figure is finding the roots of Equation (2), but re-arranged in a way Taylor Knapp found to eliminate $\sin^2(\Delta\Phi)$'s inverse dependence on $\sin(\theta_1)$ and $\sin(\theta_2)$, this method was introduced as roots of $\sin(\theta_{1,2})$ lead to discontinuities in $\sin^2(\Delta\Phi)$ so the cubic spline is ill-defined near those roots – hence the large number of roots seen in Figure 4 found by evaluating $\sin^2(\Delta\Phi)$ solely. While the re-arranged version of Equation (2) is faster to evaluate, we see that sometimes it gives too many (or too few) roots compared to the roots we find evaluating the entire, original expression in Equation (2). We still have more investigation to do here, but it seems the older version of the equation is more consistent to work with. Secondly, as just mentioned $\sin^2(\Delta\Phi)$ seems to have many roots, upon further inspection I realized a lot of these roots were very similar in value and what I hypothesized to be results of the cubic spline having trouble fitting a function with multiple discontinuities. Figure 5 shows this somewhat clearly.

When trying to solve this "spurious roots" issue I noticed a trend in every scenario I plotted, the roots of $\sin^2(\Delta\Phi)$ that weren't at discontinuities due to the other terms were always bounded by the roots of $\sin^2(\theta_1)$ and $\sin^2(\theta_2)$. In Figure 5, for example, the continuous section of the blue curve is bounded by $\sin^2(\theta_1)$'s first root and $\sin^2(\theta_2)$'s second root. Not only was this continuous section bounded nicely, it seems, but the roots inside it were the same roots that the spline of Equation (2) was finding. Thus, we thought to only apply the spline to this bounded region of $\sin^2(\Delta\Phi)$ and see if the roots found from that matched the roots we got from evaluating the spline of all of Equation (2). Taking this approach we have found that in most cases the roots found by evaluating Equation (2) as a whole and evaluating a spline of $\sin^2(\Delta\Phi)$ on this bounded region are equal, but there are always a few cases where there is a mismatch in the number of roots found between the two methods. In every case we find two roots when evaluating Equation (2), but sometimes we find less than or more than two roots evaluating only $\sin^2(\Delta\Phi)$ on the bounded region. Upon further inspection it seems all these cases are due to the spline still starting to blow up near the bounds due to discontinuities in the function at those bounds causing spurious roots, or in other cases the spline is cutoff and excludes points where there should be a found root due to the resolution of the grid interpolated on; the true root is too close to a discontinuity and thus the point is not included in the spline. While more grid points improves this issue, it comes at the cost of long run-times that we have been trying to avoid. Possible fixes to this will be discussed in the next section.

Lastly, I looked to see if specific initial conditions led to a mismatch between the roots of $\sin^2(\Delta\Phi)$ on the bounded region and Equation (2). The corner plot in Figure 6 in-

cludes the initial parameters of 10,000 randomly sampled binary NS set-ups; there is no obvious trend showing a set of parameters that causes a mismatch between roots.

VI. CHALLENGES AND NEXT STEPS

The main challenge so far has been dealing with such a sensitive function, the spline of $\sin^2(\Delta\Phi)$. Even imposing the bounds on the spline required lots of fine-tuning to stop the spline from blowing up near these boundaries, and the seemingly only reason for a failure to find consistency between these root-finding methods is numerical limits. Ideally, we would also be able to prove that these roots are bounded as described. To get around these issues we are looking at using the roots of $\sin^2(\theta_{1,2})$ in mis-matched cases; we also need to see if Taylor Knapp's re-arranged version works better in this bounded method; lastly we want to see if a different interpolator improves root-finding in the bounded method.

[1] S. W. Hawking and W. Israel, eds., *Three Hundred Years of Gravitation* (Cambridge University Press, 1989).

[2] D. Gerosa, G. Fumagalli, M. Mould, G. Cavallotto, D. P. Monroy, D. Gangardt, and V. De Renzis, Efficient multi-timescale dynamics of precessing black-hole binaries, Phys. Rev. D **108**, 024042 (2023), arXiv:2304.04801 [gr-qc].

[3] A. Einstein and N. Rosen, On gravitational waves, Journal of the Franklin Institute **223**, 43 (1937).

[4] B. P. e. a. Abbott (LIGO Scientific Collaboration and Virgo Collaboration), Observation of gravitational waves from a binary black hole merger, Phys. Rev. Lett. **116**, 061102 (2016).

[5] T. A. Apostolatos, C. Cutler, G. J. Sussman, and K. S. Thorne, Spin-induced orbital precession and its modulation of the gravitational waveforms from merging binaries, Phys. Rev. D **49**, 6274 (1994).

[6] Sounds of Spacetime, Spinning binaries: Exploring spin and precession, `https://www.soundsofspacetime.org/spinning-binaries.html`, accessed: April 25, 2026.

[7] C. L. Rodriguez, M. Zevin, C. Pankow, V. Kalogera, and F. A. Rasio, Illuminating Black Hole Binary Formation Channels with Spins in Advanced LIGO, Astrophys. J. Lett. **832**, L2 (2016), arXiv:1609.05916 [astro-ph.HE].

[8] C. M. Will, Inaugural Article: On the unreasonable effectiveness of the post-Newtonian approximation in gravitational physics, Proceedings of the National Academy of Science **108**, 5938 (2011), arXiv:1102.5192 [gr-qc].

[9] D. Gerosa, M. Kesden, U. Sperhake, E. Berti, and R. O'Shaughnessy, Multi-timescale analysis of phase transitions in precessing black-hole binaries, Phys. Rev. D **92**, 064016 (2015), arXiv:1506.03492 [gr-qc].

[10] É. Racine, Analysis of spin precession in binary black hole systems including quadrupole-monopole interaction, Phys. Rev. D **78**, 044021 (2008), arXiv:0803.1820 [gr-qc].

[11] A. Klein, Efpe: Efficient fully precessing eccentric gravitational waveforms for binaries with long inspirals (2021), arXiv:2106.10291 [gr-qc].

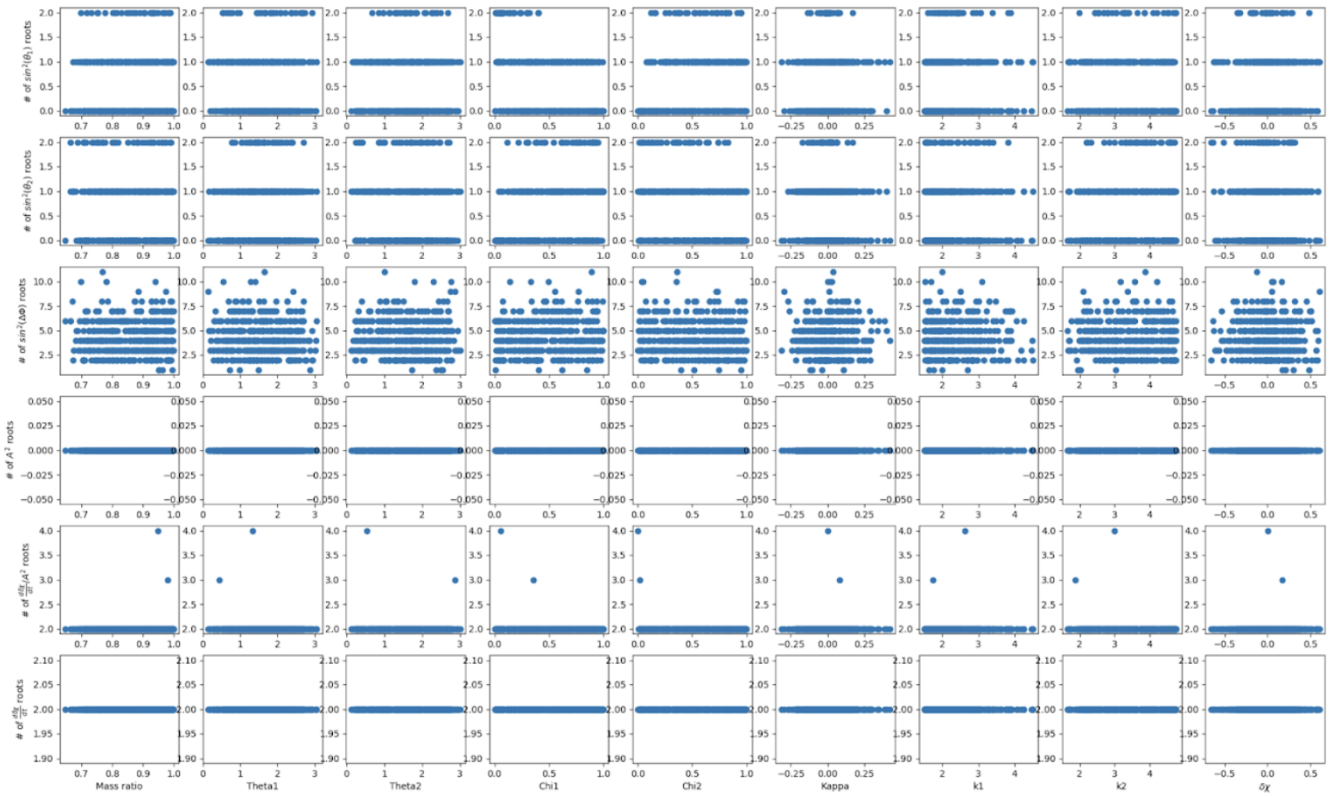


FIG. 4. Each row is the roots of a different factor of $\frac{d\delta\chi}{dt}$, the last row is the roots of $\frac{d\delta\chi}{dt}$ found by evaluating a cubic spline on the entire expression, the second to last row is the roots found by evaluating a cubic spline on Taylor Knapp's rearranged version of Equation (2) – more on that below. The number of roots from each term is plotted against each initial parameter that determines the evolution of the system. As can be seen $\mathcal{A}^2$ always has no roots, thus can be ignored in the future.

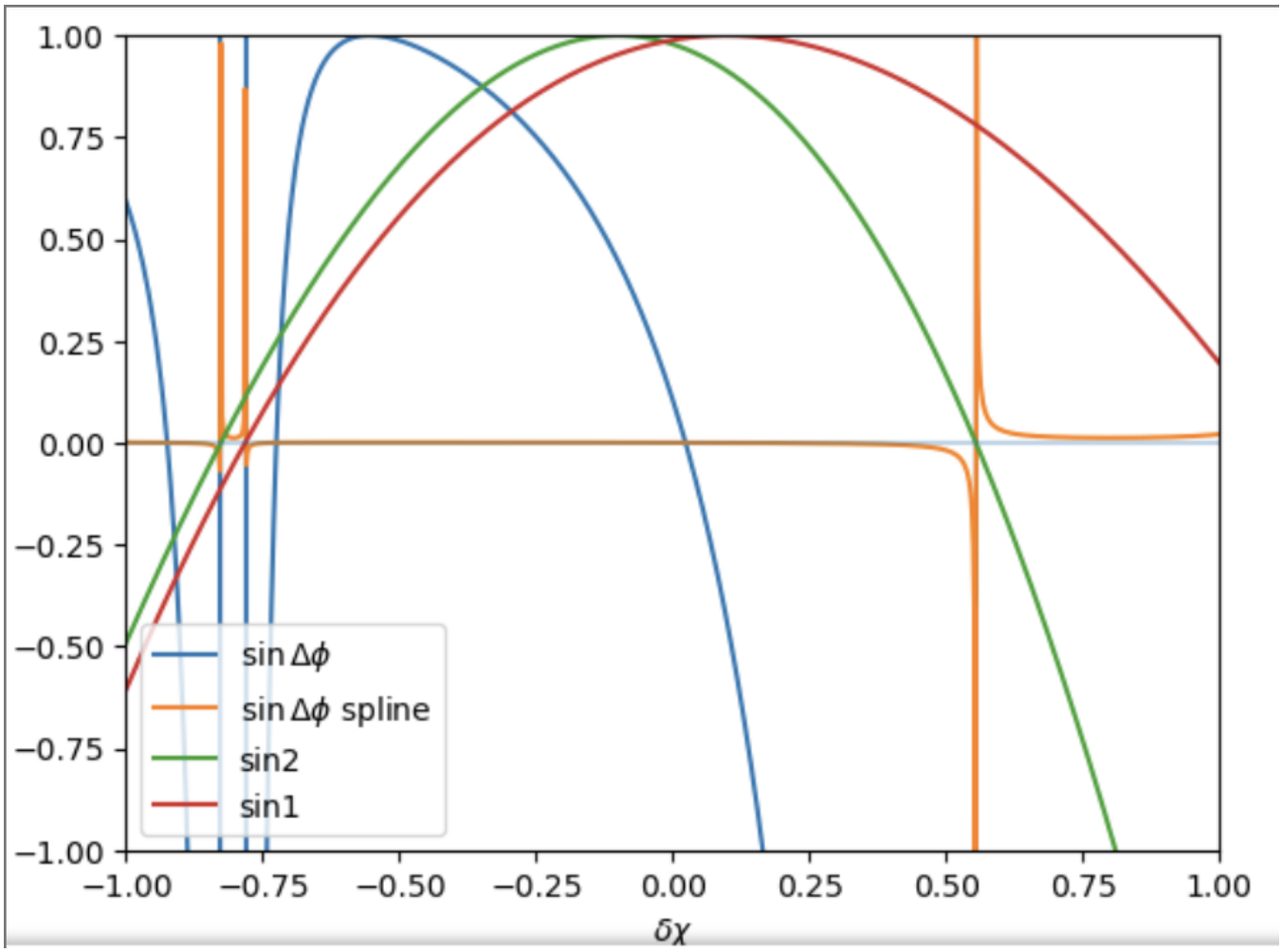


FIG. 5. Graphs of $\sin^2(\theta_1), \sin^2(\theta_2)$ and the analytical and spline fit of $\sin^2(\Delta\Phi)$ over a grid of $\delta\chi$ values from -1 to 1. As can be seen the spline of $\sin^2(\Delta\Phi)$ does not match the analytical form of it, and where $\sin^2(\theta_1)$ and $\sin^2(\theta_2)$ have roots the spline fits the clear discontinuity in $\sin^2(\Delta\Phi)$ by spiking negative then positive or positive then negative, leading to returned roots at those points even though they are artifacts of a discontinuity at those points.

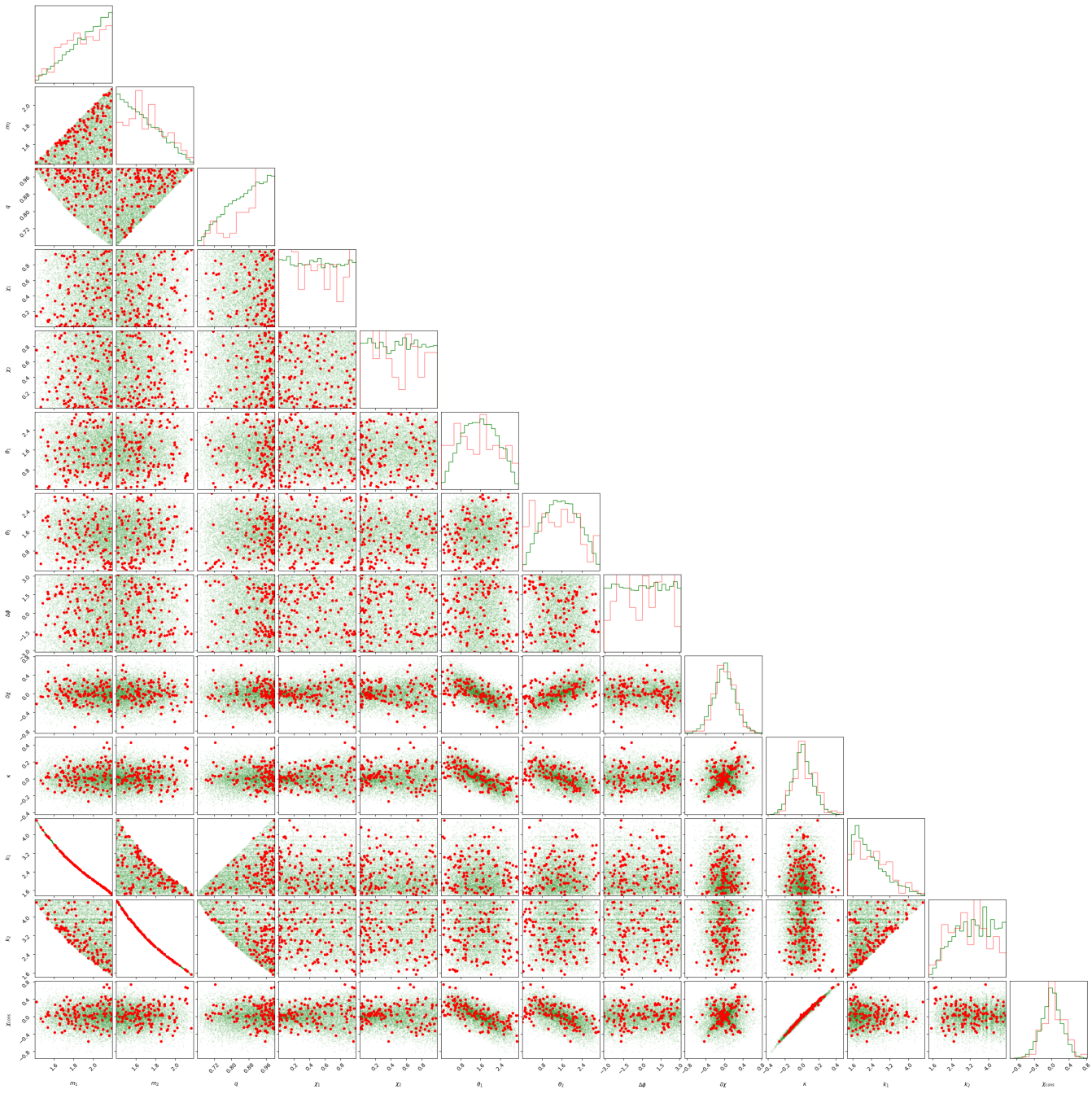


FIG. 6. In light green are all 10,000 scenarios, in red are the 123 scenarios that had a mismatch between roots found by evaluating Equation (2) as a whole and by evaluating $\sin^2(\Delta\Phi)$ on the bounded region. Although dense, there seems to be no collection of "bad" scenarios in regions of a specific parameter, or pair of parameters, indicating that this is a numerical, not physical, issue.